energies

MDPI

Article

An Analysis of a Laminar-Turbulent Transition and Thermal Plumes Behavior in a Paramagnetic Fluid Subjected to an External Magnetic Field

Anna Kraszewska * and Janusz Donizak

Department of Fundamental Research in Energy Engineering, AGH University of Science and Technology, 30 Mickiewicza Av., 30-059 Krakow, Poland; janusz.donizak@agh.edu.pl
* Correspondence: anna.kraszewska@agh.edu.pl; Tel.: +48-12-617-26-62

Abstract: Transition to turbulence and changes in the fluid flow structure are subjects of continuous analysis and research, especially for unique fields of research such as the thermo-magnetic convection of weakly magnetic fluids. Therefore, an experimental and numerical research of the influence of an external magnetic field on a natural convection's fluid flow was conducted in the presented research. The experimental part was performed for an enclosure with a 0.5 aspect ratio, which was filled with a paramagnetic fluid and placed in a superconducting magnet in a position granting the enhancement of the flow. The process was recorded as temperature signals from the thermocouples placed in the analyzed fluid. The numerical research enabled an investigation based not only on temperature, but velocities as well. Experimental and numerical data were analyzed with the application of extended fast Fourier transform and wavelet analysis. The obtained results allowed the determination of changes in the nature of the flow and visualization of the influence of an imposed strong magnetic field on a magnetic fluid. It is proved that an applied magnetic field actuates the flow in Rayleigh-Benard convection and causes the change from laminar to turbulent flow for fairly low magnetic field inductions (2T and 3T for $\Delta T = 5$ and 11 °C respectively). Fast Fourier transform allowed the definition of characteristic frequencies for oscillatory states in the flow, as well as an observation that the high values of magnetic field elongate the inertial range of the flow on the power spectrum density. Temperature maps obtained during numerical simulations granted visualizations of thermal plume formation and behavior with increasing magnetic field.

Keywords: thermo-magnetic convection; transition to turbulence; paramagnetic fluid

Citation: Kraszewska, A.; Donizak, J. An Analysis of a Laminar-Turbulent Transition and Thermal Plumes Behavior in a Paramagnetic Fluid Subjected to an External Magnetic Field. *Energies* **2021**, *14*, 7972. https://doi.org/10.3390/en14237972

Academic Editor: Andrea Mariscotti

Received: 29 October 2021
Accepted: 23 November 2021
Published: 29 November 2021

1. Introduction

As natural convection is one of the most common processes occurring in the environment, the heated from below configuration has been studied intensively in the literature—both from the application point of view (to suppress or enhance heat transfer and fluid motion) and to delve into the theory of the phenomenon [1–6]. Trying to manage natural convection is another interesting field of research. One of the ways to achieve some kind of control over this process is to introduce another force into the system—by using fluids with magnetic properties located in the magnetic field.

That field of research was initiated by a few main events in the research area. In 1820 Oersted discovered that a magnetic field exists around an electric current flowing through a wire and Biot and Savart demonstrated that the magnetic induction is proportional to that electric current (later Whittaker obtained a relation known today as the Biot-Savart law [7]). Twenty seven years later Faraday [8] found that every substance has magnetic properties and classified them into paramagnetic and diamagnetic groups. A century later, a discovery of conductors operating above the boiling point of liquid nitrogen [9] enabled the construction of superconducting magnets and studies concerning a new field of research—thermo-magnetic convection in weakly magnetic fluids. In 1991 Braithwaite [10]

researched the influence of a strong magnetic field on paramagnetic fluids and provided a mathematical description of forces acting on a fluid with temperature differences. Huang published a paper [11] reporting a possibility of suppressing or enhancing heat transfer in a paramagnetic fluid. The development of super-computers happening at the same time provided the opportunity to model and solve those complicated problems. Ozoe published "Magnetic convection" [12]—the result of long-term research. Tagawa [13–15] studied the numerically magnetic convection of air and water in a cubical enclosure proving that weak magnetic fluids can be greatly influenced by the magnetic field. Bednarz [16–18] investigated the influence of different configurations of thermally active walls in magnetic convection and provided the first qualitative visualizations of the temperature field in the central vertical plane using particle image thermometry. The above studies provide a major contribution as a Nusselt number information and its changes with the magnetic field applied, as well as some basic flow visualizations.

Many other geometrical configurations were studied, e.g., coaxial cylinders [19], porous media [20], thermosyphons [21,22] as well as forced thermo-magnetic convection [23]. A new topic in the field started in the 2000s concerning nano-fluids with magnetic properties and their behavior under the influence of the strong magnetic field [24–28].

Those studies, in general, provided much useful information about integral heat transfer, but in steady and laminar conditions. Szabo and Fruh [29] analyzed numerical transition from natural convection to thermomagnetic convection in a square enclosure for small values of magnetic induction (up to 1T) for a heated from the sides configuration and described the formulation of side thermal plume with increasing magnetic influence. Pyrda, Wróbel and Kenjeres [30–32] undertook the subject of extending the analysis of thermo-magnetic convection in the Rayleigh-Benard configuration to the transitional and turbulent regimes for a cubical enclosure. They provided detailed insight into the fluid flow and heat transfer changes under the influence of an external magnetic field over a range of parameters (different Prandtl numbers and values of imposed magnetic field 0–15T) and determined three flow regimes: a transient regime ($Ra_{TM} \leq 3 \times 10^7$), a regime where a thermo-magnetic mechanism dominates ($3 \times 10^7 < Ra_{TM} \leq 3 \times 10^8$), and an additional wall heat transfer regime for $Ra_{TM} \geq 3 \times 10^8$. Additionally, they presented basic information about the evolution of thermal plumes and coherent structures with increasing strength of the magnetic field showing the dynamizing action of the imposed magnetic field. The transition from laminar to turbulent flow was determined as 3×10^7 for cubical geometry, and 4×10^7 to 1.3×10^8 for a tall enclosure (aspect ratio AR = height/width = 2) [33]. A comparison of thermo-magnetic convection, heat transfer and basic spectral analysis for vessels with aspect ratios 0.5 and 2.0 for the experimental results was presented in [34], indicating that the heat transfer enhancement, as well as fluid flow structure, strongly depends on the geometry height.

The goal of the proposed research is to significantly extend the research of laminar-turbulent transition in a thermo-magnetic convection. As reported, the works focused on the cubical cavity. To the authors best knowledge there are no combined experimental and numerical analyses of transitional flow in a geometry with an aspect ratio of 0.5, therefore the main purposes of the presented work are as follows:

- To identify the laminar-turbulent transition of the fluid flow in a shallow geometry in the thermo-magnetic convection
- The performing of a traditional visualization of the flow field in the experimental part—to try to visualize the flow changes performing the wavelet transform—a technique not applied to thermo-magnetic convection before
- To provide quantitative information about characteristic frequencies from fast Fourier transform of the temperature and velocity signals
- To deliver a benchmark case for further analysis in the absence of energy spectrum analyses for the experimental and numerical thermo-magnetic convection process in the transitional state

- To describe the evolution and behavior of thermal plumes when under the influence of imposed, strong magnetic gradients.

2. Theoretical Outline

A motion of the fluid in the natural convection process is a result of gravitational force acting on a fluid:

$$\mathbf{f^g} = \mathbf{g}\rho \tag{1}$$

$$\mathbf{f^G} = \mathbf{g}(\rho - \rho_0) \tag{2}$$

and since a fluid density depends on a temperature, the value of the gravitational force influencing the fluid will strongly differ with temperature. Taking note of the Boussinesq model, which states that the density of the fluid can be assumed constant for small differences of the temperature, except for the buoyancy force [35], the expression for the density comes as follows:

$$\rho \simeq \rho_0(1 - \beta(T - T_0)) \tag{3}$$

So the buoyancy force can be expressed as:

$$\mathbf{f^G} = -\mathbf{g}\rho_0\beta(T - T_0) \tag{4}$$

This explains the natural phenomenon which occurs widely in nature—in the presence of a gravitational field—cold fluid will move downwards and the hot one will rise.

A similar effect can be achieved in the magnetic realm—by applying an external magnetic field to the fluid with specific magnetic properties—as in natural convection. The magnitude of the fluid reaction to the magnetic field can be connected with volume magnetic susceptibility:

$$\chi_v = \mathbf{M}/\mathbf{H} \tag{5}$$

and mass magnetic susceptibility:

$$\chi = \chi_v/\rho \tag{6}$$

So the magnetic force acting on a fluid can be written as:

$$\mathbf{f^{mg}} = \mu_0(\mathbf{M}\cdot\nabla)\mathbf{H} \tag{7}$$

As the magnetic induction b depends on the intensity of a magnetic field and on a magnetic permeability of the material, and also that for a paramagnetic fluid $\chi << 1$, the equation for the magnetic force can be also written as:

$$\mathbf{f^{mg}} = \frac{\chi}{2\mu_0}\nabla\mathbf{b}^2 \tag{8}$$

Utilizing the above relation and Curie's law for paramagnetic materials, which states that for the fixed value of the magnetic field, the material's magnetic susceptibility is inversely proportional to temperature, Tagawa et al. developed an equation to describe the magnetic buoyancy force [15]:

$$\mathbf{f^M} = -\left(1 + \frac{1}{\beta T_0}\right)\frac{\chi_0\rho_0(T - T_0)}{2\mu_0}\nabla\mathbf{b}^2 \tag{9}$$

This directly indicates that the fluid particles, which have paramagnetic properties, are attracted to the square of a magnetic field's gradient if their temperature T is lower than the reference temperature T_0. Therefore, to achieve the intensification of the fluid motion, the experimental enclosure filled with paramagnetic fluid was placed in the upper half of the superconducting magnet's working section, so the gravitational and magnetic forces were acting in the same direction, as schematically shown in Figure 1.

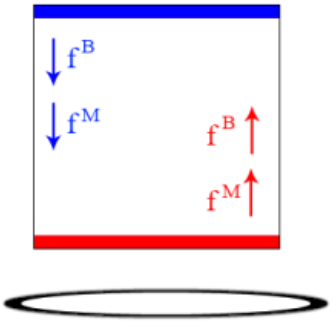

Figure 1. A schematic view of the buoyancy and magnetic forces acting on a fluid in the present research.

3. Experimental Setup

The experimental setup used in this work is shown in Figure 2. It consisted of an experimental enclosure (Figure 3) designed to have a specific aspect ratio (AR = height/width) of 0.5 filled with experimental fluid and placed in the bore of a superconducting magnet.

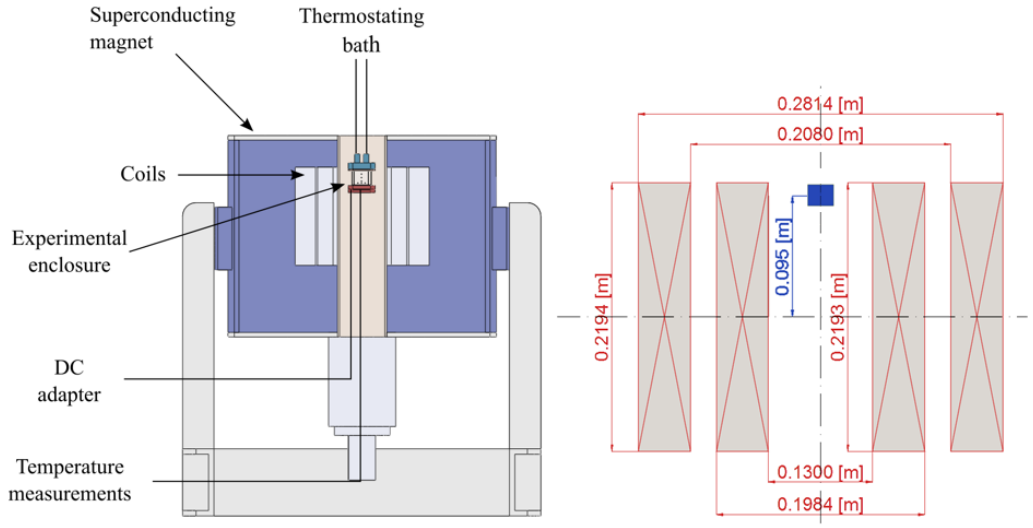

(**a**) (**b**)

Figure 2. A schematic view of the experimental setup (**a**) and dimensions of the magnet's coils (**b**).

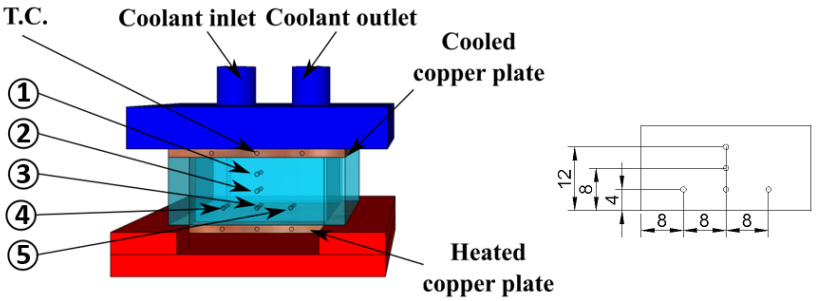

Figure 3. Experimental enclosure and exact placement of the thermocouples in the working fluid.

Four vertical walls of the experimental vessel were constructed from Plexiglass and insulated with a sponge, whereas the horizontal walls consisted of copper plates, which were heated with a nichrome wire connected to a DC supply from the bottom, and isothermally cooled from the top (with cold water supplied from the thermostatic bath). Five thermocouples were inserted directly through one Plexiglas wall into the fluid (6 mm in depth). The placement of the thermocouples is shown in Figure 3. To control the temperature of

the thermally active walls in this Rayleigh Benard configuration, six more thermocouples were placed in the copper plates (three thermocouples in each).

The experimental enclosure, filled with fluid, was then placed in the bore of a superconducting magnet (Figure 2). In order to achieve intensification of the heat transfer and to increase fluid motion to observe the change in flow characteristics, a position of the experimental enclosure in the bore of a superconducting magnet was chosen carefully. As the intensification of the fluid motion will appear if the magnetic and buoyancy forces will act in the same direction (as shown in Figure 1) for paramagnetic fluid, the enclosure was placed in the upper part of the superconducting magnet's bore.

To calculate the magnetic field distribution and its gradient, here are the current densities in the internal and external coils, respectively: 140.9×10^{-6} A/m^2 and 167.3×10^{-6} A/m^2 (for the maximum value of the magnetic induction 10T).

The fluid used in this research was a 50% volume glycerol aqueous solution. Since both water and glycerol have diamagnetic properties, an addition of 0.8 mol/(kg of solution) of gadolinium nitrate hexahydrate $Gd(NO_3)3{\cdot}6H_2O$ crystals was made to make them paramagnetic. The fluid properties are presented in Table 1.

Table 1. Properties of the working fluid.

Property	Value	Unit
Heat capacity c_p	2.92×10^3	J/kgK
Thermal diffusivity α	9.13×10^{-8}	m^2/s
Thermal expansion coefficient β	1.21×10^{-5}	1/K
Dynamic viscosity μ	1.30×10^{-2}	kg/ms
Thermal conductivity λ	0.376	W/mK
Kinematic viscosity ν	9.25×10^{-6}	m^2/s
Density ρ	1411	kg/m^3
Mass magnetic susceptibility χ_m	2.39×10^{-7}	m^3/kg

The experimental procedure consisted of two main stages. The first one was connected with the thermal analysis and involved the estimation of the heat losses from the experimental enclosure. This was essential to calculate the Nusselt number (for the mathematical procedure see the Ozoe and Churchill method [26,36]). In order to estimate the heat losses, the experimental enclosure was filled with distilled water and installed in the magnet's working section but in reversed Rayleigh-Benard configuration so that the cooled wall was on the bottom and the heated one on the top. This created conditions to achieve only conduction in the fluid inside the enclosure, but in reversed Rayleigh-Benard configuration without convective fluid motion. Next the temperature on the thermally active walls was set. The bottom wall temperature was constant (18 degrees Celsius), as was the temperature in the magnets working section. The temperature on the top wall was changed seven times, in the range from 21 to 38 degrees. For every temperature, after the thermal stabilization of the system, the heating power was measured at the top wall. With the assumption of temperature stratification and strict conduction conditions, the heat flux can be calculated directly from Fourier's law. The difference between the calculated heat flux and the one measured at the heated wall is the heat loss.

The next step in the analysis was connected with measurements of the temperature changes in the working fluid in natural convection and the thermo-magnetic convection processes. Therefore, the experimental enclosure was filled with working fluid and placed in the magnet's working section in proper Rayleigh-Benard configuration with the bottom wall heated. Then, the temperature on the thermally active walls was set. As mentioned, the temperature on the cold wall was almost constant during all experiments and it was 18 degrees, while on the hot wall two sets of temperature were analyzed: 23 °C and 29 °C. For every temperature difference eleven measurements were done—one without the external magnetic field present (natural convection case) and ten measurements for the different magnetic inductions—from 1 T to 10 T. For every case, when the setup was

thermally stable, changes in the fluid temperature from five thermocouples were recorded during 15 min periods with 0.3 s frequency.

4. Numerical Procedure

The phenomenon of Rayleigh-Bénard thermo-magnetic convection has been simulated based on the fundamental laws of physics: Maxwell's equations of stationary magnetic field and nonstationary non-isothermal equations of fluid flow.

4.1. Magnetic Field Calculations

The governing equations of stationary magnetic field can be developed from Maxwell (equation [37]):

$$\nabla \times \mathbf{H} = \mathbf{J} \tag{10}$$

$$\mathbf{b} = \nabla \times \mathbf{A} \tag{11}$$

$$\mathbf{b} = \mu_0(1 + \chi_v)\mathbf{H} \tag{12}$$

where **H** denotes a vector of the magnetic field strength, the vector of the magnetic induction b is proportional to a vector of the magnetic field strength. The source of the magnetic field in our experimental setup is represented by a vector of electric current density **J** flowing thru the electromagnet coils. Symbol **A** expresses a vector of a magnetic potential. The above set of equations can be reduced into the single vector equation called the Ampere's law

$$\nabla \times \left((\mu_0(1 + \chi_v))^{-1} \nabla \times \mathbf{A} \right) = \mathbf{J} \tag{13}$$

which accomplished with boundary condition (the decay of the magnetic field in the far distance from field source)

$$\mathbf{n} \times \mathbf{A} = 0 \tag{14}$$

imposed of the surface of the large sphere enclosing electromagnet (**n** is a normal vector to the sphere surface) forms a complete mathematical model of the stationary magnetic field. The task is to solve Ampere's equation with regard to the distribution of the a vector of magnetic potential, and to recalculate the results into a distribution of magnetic induction vector b in the domain of interest.

Ampere's equation has been solved applying a second order numerical scheme using a finite element discretization of the sphere of 10 m diameter. The size of the finite elements were proportionally growing with the radius of a sphere in order to obtain a much better approximation of the field strength in the center of the electromagnet. The input data describing the distribution of the current density within the system of coils are evaluated from electromagnet technical instruction.

4.2. Nonisothermal Flow Field

The single phase flow field equations with volumetric force (as a sum of gravity and magnetic buoyancy forces) were solved for the 2D section of the cube described in the experimental setup section of the paper. Material properties of the fluid together with the boundary condition imposed followed the experimental measurements. Nonstationary simulation was carried out on the long time distance starting from the pure conduction temperature and stagnant flow condition. The time step of second order numerical scheme (backward differences) was imposed 10^{-3} sec. which allowed for the keeping of the courant number below 0.05. Spatial distribution of unknown velocity and temperature were obtained for the set of second order finite elements net of the size 200×100 (horizontal and vertical number of rectangular elements), which ensured the high resolution of the solution allowing to observe the changes in the character of the thermal plumes. The results of the simulations were stored for every 0.1 sec of the simulation period.

5. Analysis Methodology

Temperature signals were then analyzed. Fast Fourier transform and wavelet analysis were applied for all thermocouples placed in the working fluid. Those analyses were done for fluctuations of the temperature, but not for the raw temperature signals.

Spectral analysis was obtained through the fast Fourier transform (FFT), which computes the discrete Fourier transform (DFT) of a sequence [38]:

$$F_n = \sum_{i=0}^{N-1} x_i e^{-\frac{2\pi i}{N} ni} \tag{15}$$

As the experimental measurements delivered only temperature information (the experimental setup is too small to measure velocity in our conditions), temperature is the most important aspect of this analysis, but the spectral functions of a scalar field (temperature) are very useful tools in analysing the transport mechanism in moving fluid. Thus, power density or spectrum may be calculated with the utilization of FFT:

$$\text{Power density}\left(e^{j\omega}\right) = \sum_{m=-\infty}^{\infty} r_{xx}(m) e^{-j\omega m} \tag{16}$$

With the use of the peridogram method, which estimates power as time-integral square amplitude (TISA) from amplitude obtained with FFT:

$$\text{Power density (TISA)} = \frac{\Delta t\left(\text{Real}^2 + \text{Imaginary}^2\right)}{n} \tag{17}$$

The spectral functions of temperature usually depend on viscosity, thermal diffusivity and energy dissipation, but in some frequency ranges those functions do not depend on diffusion processes [39]. This frequency subrange is known as the inertial-convective region, and in this range spectral functions tend to have an inclination of a wave number with $-5/3$ exponent.

For numerical results, the FFT analysis was done both for temperature and velocity signals.

The second form of signal analysis in the presented study is the wavelet analysis. It is a mathematical method introduced by Morlet in 1982 [40]. It is a method similar to Fourier transform, but provides more information. In the wavelet theory the shape of the primary wavelet function changes with frequency in the time domain to ensure the best possible fitting to irregular signal data. Moreover, while the Fourier transform provides information in the global frequency domain, the wavelet transform identifies where a certain frequency exists in the temporal or spatial domain.

The widely used one-dimensional continuous wavelet transform is defined as [41]:

$$C_{a,b} = \int_R x(t) \frac{1}{\sqrt{a}} \psi\left(\frac{t-b}{a}\right) dt \tag{18}$$

where $x(t)$ is the input signal, ψ is the wavelet function, a is the scale, b is the position and $C_{a,b}$ is the continuous wavelet coefficient. Parameters a and b are used to fit the shape and location of the wavelets to the original signal. Parameter a is responsible for the compression or stretching of the mother wavelet, while b corresponds to the movement of the time localization center through all data point.

In this study a Mexican hat wavelet was used:

$$\psi(x) = \frac{2}{\sqrt{3}} \pi^{-1/4} (1 - x^2) e^{-x^2/2} \tag{19}$$

6. Results

6.1. Temperature Signals

As the experimental and numerical studies generated a fair amount of results, only selected cases will be fully presented in this paper. All of the analyses below were performed for the bottom middle placement of the thermocouple in the experimental enclosure (TC4 in Figure 3).

Figures 4 and 5 present temperature fluctuations from the experimental and numerical research for both temperature differences and for the magnetic inductions for 0 T (the natural convection case) and $\mathbf{b}_{0MAX}$ = 1–5, 9 T. For almost all cases the characters of the temperature fluctuations are similar in the experimental and numerical approach. The difference in temperature fluctuations magnitude is possibly explainable by the thermocouple accuracy (+/−1.1–2.2 °C in range 0–275 °C) and its temperature inertia, as well as the fact that the thermocouples used in the experimental research were type K (NiCr-NiAl), and while aluminum and chromium have paramagnetic properties, the nickel is a ferromagnet and may be strongly influenced by the strong magnetic field. Unfortunately, the specification of the experimental setup does not allow for an easy apparatus modification, therefore the experimental results are mainly to confirm characters of the observed and analyzed processes.

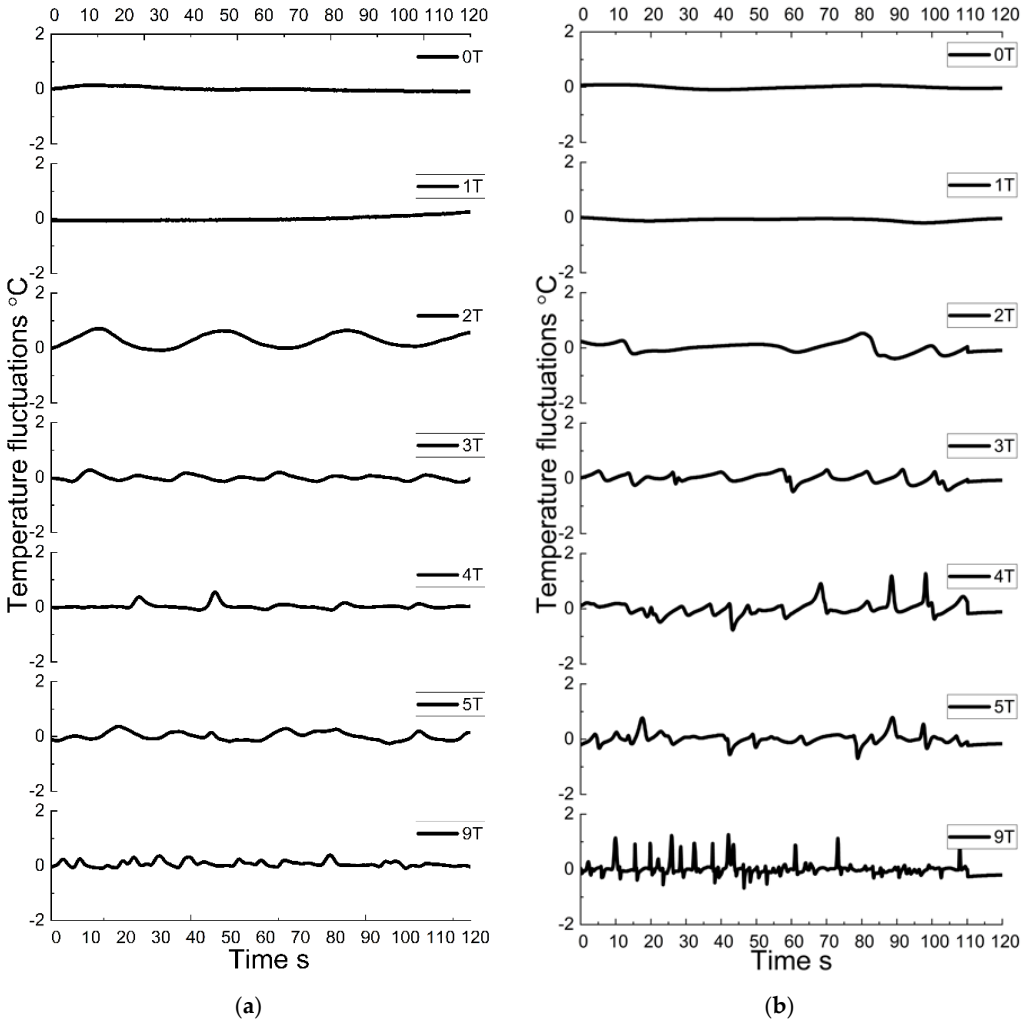

Figure 4. Temperature fluctuations for the case with ΔT = 5 °C—(**a**) experimental and (**b**) numerical.

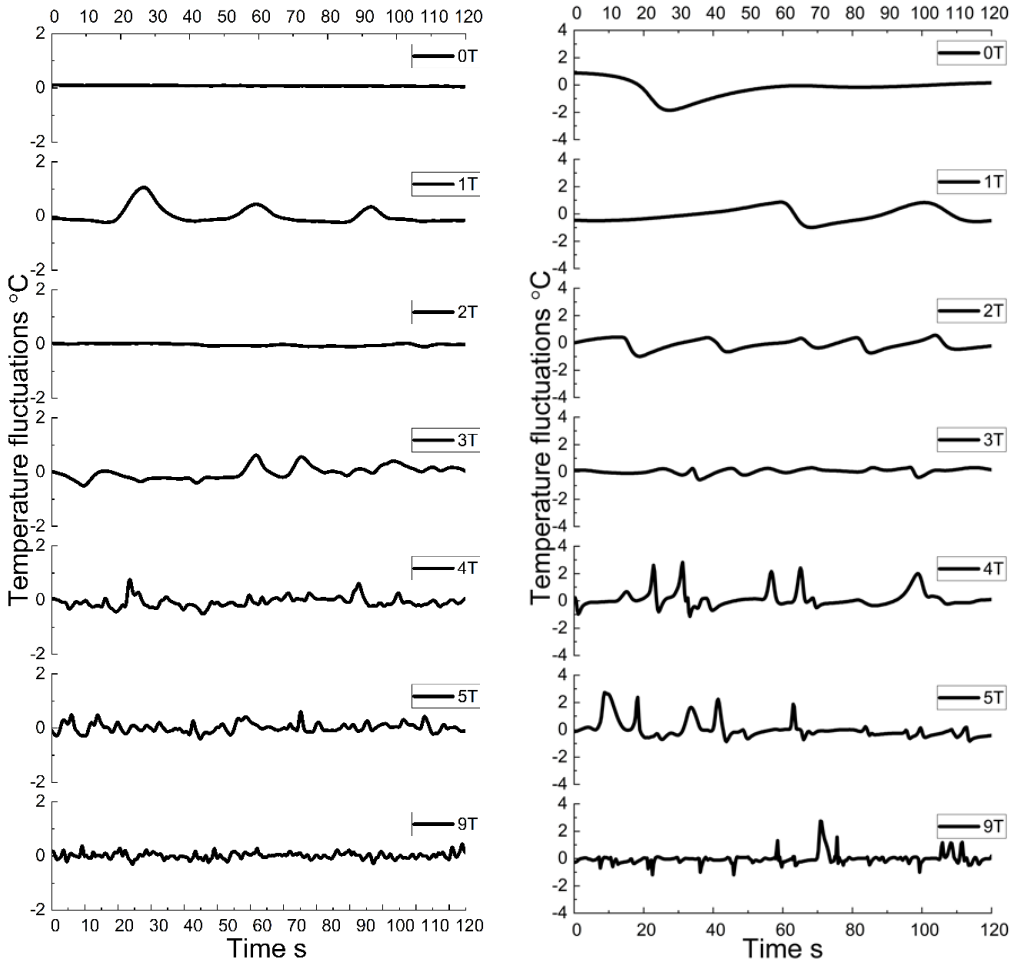

Figure 5. Temperature fluctuations for the case with ΔT = 11 °C—(**a**) experimental and (**b**) numerical.

In natural convection cases the temperature lines are flat and only in the numerical ΔT = 11 °C case does the line show single slow fluctuation. The thermal Rayleigh number is 8.22×10^4 for the smaller temperature difference and 2.21×10^5 for the higher temperature difference, which indicates that the flow is steady. The laminar and the studied enclosure have a dominant convection cell that fills a greater part of the enclosure. The same behavior is observed for ΔT = 5 °C and $\mathbf{b}_{0MAX}$ = 1T. A significant change occurs for the magnetic field induction of 2T for ΔT = 5 °C and $\mathbf{b}_{0MAX}$ = 1T in ΔT = 11 °C. The lines representing the temperature changes become unstable and small, periodic fluctuations can be observed. Those fluctuations alone may suggest that a thermal plume is slowly arising from the heated wall—a process where hot fluid from the bottom has to rise up and an interplay emerges between the two forces: the buoyancy effect that tries to push the hot fluid upward and the inertia effect induced by the convective cell that opposes an upward motion. This phenomenon is clearly visible in Section 6.2, which will be discussed later.

According to [42], three regimes can de distinguished based on the thermo-magnetic Rayleigh number: transient regime ($Ra_{TM} \leq 3 \times 10^7$), a regime where the thermo-magnetic mechanism dominates ($3 \times 10^7 < Ra_{TM} \leq 3 \times 10^8$), and an additional wall heat transfer regime for $Ra_{TM} \geq 3 \times 10^8$. Therefore, the fluctuations in temperature signals ($\mathbf{b}_{0MAX}$ = 2T for ΔT = 5 °C and $\mathbf{b}_{0MAX}$ = 1T in ΔT = 11 °C) indicate that the flow is in the transient regime—flow structure changes. There are more convective cells in the analyzed volume and the velocity starts to increase. A further rise of the magnetic induction, for both cases of temperature differences, causes the growth of fluctuation frequency. For the maximal value of the magnetic induction ($\mathbf{b}_{0MAX}$ = 9T), temperature signals are characterized by high

frequency fluctuations. An interesting behavior can be observed in the experimental results for ΔT = 11 °C for the magnetic field value of 2T where the temperature signal is flattened and stabilized in relation to $\mathbf{b}_{0MAX}$ = 1T. This suppression of the temperature fluctuations in a weak magnetic field was also observed in [31] where Pyrda studied thermo-magnetic convection for the same two temperature conditions in a cubical enclosure, but he observed this stabilizing influence of magnetic field in a higher temperature difference (ΔT = 11 °C).

The FFT analysis for temperature signals is presented in Figures 6–9 as amplitude-frequency graphs and a temperature power spectrum. To maintain transparency only a chosen result will be presented: for ΔT = 5 °C: $\mathbf{b}_{0MAX}$ = 0, 2, 5, 9T and for ΔT = 11 °C: $\mathbf{b}_{0MAX}$ = 0, 1, 5, 9T. This approach will allow the demonstration of the change in flow structure (transition from the laminar to the turbulent regime) caused by the addition of an external magnetic field to magnetic fluid flow.

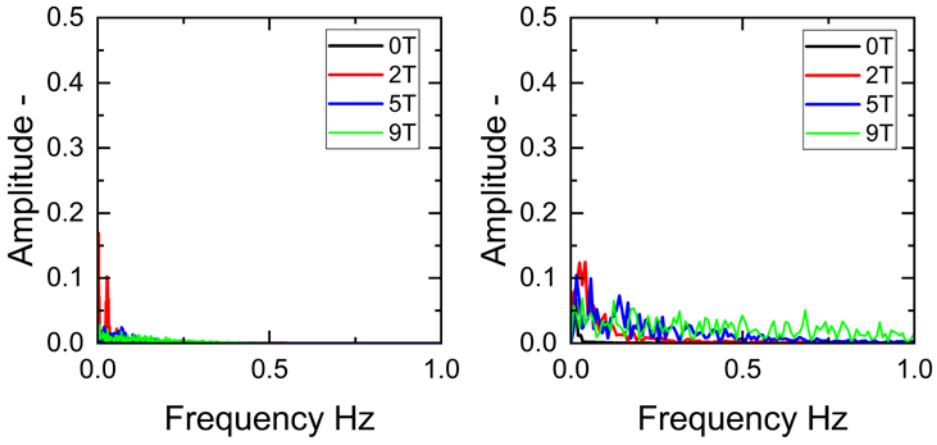

Figure 6. Fast Fourier transform of temperature results for the case with ΔT = 5 °C—(**a**) experimental and (**b**) numerical.

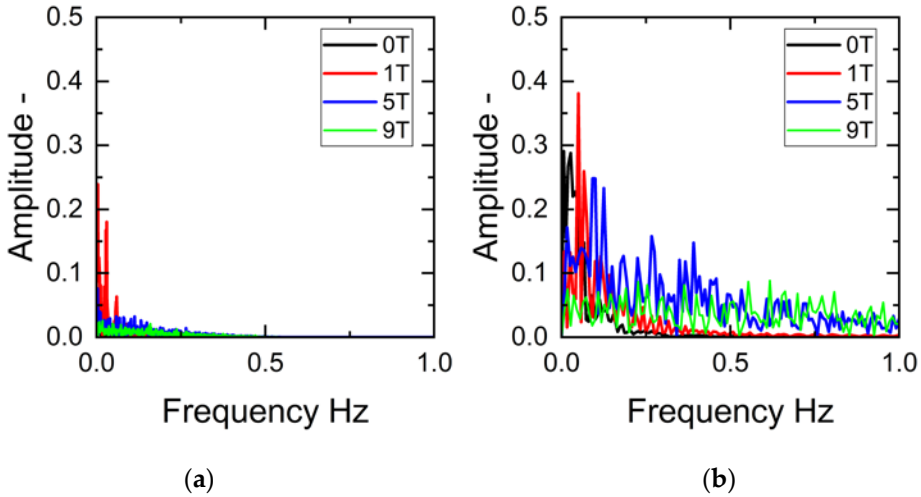

Figure 7. Fast Fourier transform of temperature results for the case with ΔT = 11 °C—(**a**) experimental and (**b**) numerical.

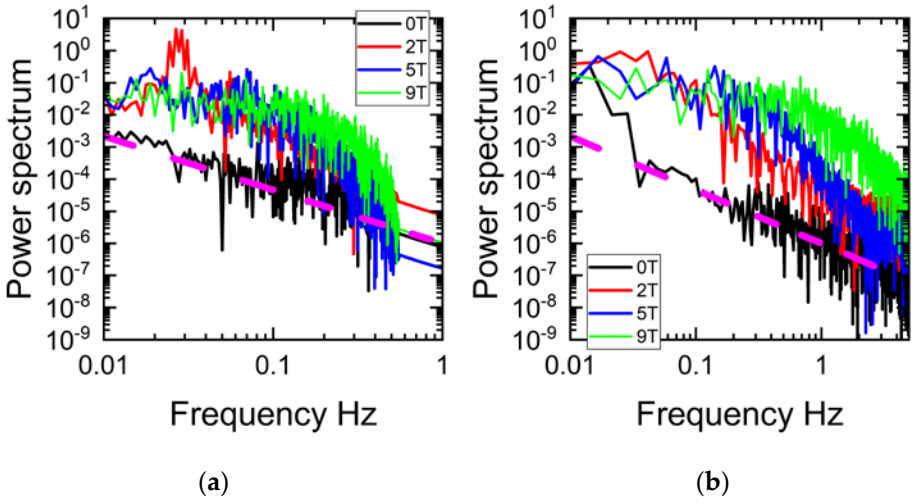

Figure 8. Power spectrum of the temperature for the case with ΔT = 5 °C (**a**) experimental and (**b**) numerical.

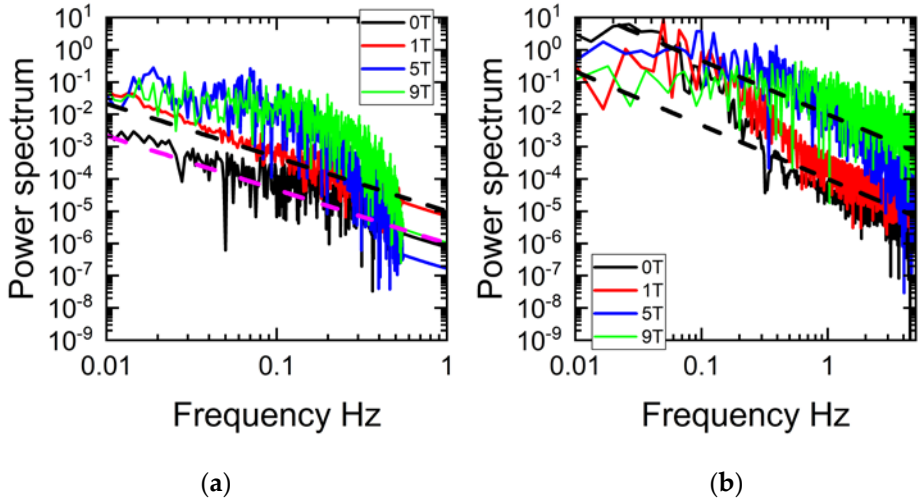

Figure 9. Power spectrum of the temperature for the case with ΔT = 11 °C (**a**) experimental and (**b**) numerical.

Figure 6 presents amplitude versus frequency for the experimental and numerical analyses for the temperature difference of 5 °C. For the natural convection case there is no distinguished peak visible, but an important change is evident for $\mathbf{b}_{0MAX}$ = 2T (the red colored peaks). The specific frequencies for this case are 0.0022 and 0.0266 [Hz] for the experiment and 0.0249 and 0.0416 [Hz] for the numerical research. For a further increase of the magnetic field, the experimental study shows many peaks with low amplitude, while in the numerical cases the magnitudes of amplitude are larger. This again may be explainable by the imperfect character of the experimental setup.

For the case of the higher temperature difference (Figure 7) the highest peaks occur for $\mathbf{b}_{0MAX}$ = 1T ($Ra_{TM} = 1.43 \times 10^7$), and the specific frequencies are 0.0044, 0.0299 and 0.0599 [Hz] for the experimental part and 0.0499 and 0.0666 [Hz] for the numerical part. A similarity to the results reported in [31] can be seen, as a specific frequency of 0.02941 was observed in the cubical enclosure in a magnetic field induction equal to 1T. In the numerical studies, the increase of the magnetic strength provides many specific peaks—it shows a nearly oscillatory character. The reasons of such results require further analysis, which will be conducted in the near future.

Power density of the temperature function is shown in Figures 8 and 9. For the smaller temperature difference between thermally active walls, both experimental and numerical

results of the power density function have the same character. For natural convection cases, functions are straight and demonstrate good match to dash lines, which represent the law of $-5/3$ exponent for the energy spectrum. Therefore, the temperature power function depends mostly on the energy and temperature dissipation. This regime is called inertial-convective [39]. Introducing magnetic field induction to the system significantly changes the characters of the functions scope—they move up and are no longer almost linear. For the experimental results in $\mathbf{b}_{0MAX}$ = 2T (red line), a distinctive peak on the power spectrum can be observed for frequency 0.0266. This clear local extremum may indicate two phenomena: transition from laminar to turbulent flow and the effect of moving periodic coherent structures. As the thermo-magnetic Rayleigh number is 2.58×10^7 for this case and the point for the laminar-turbulent transition for the thermo-magnetic convection was specified as $Ra_{TM} = 3 \times 10^7$ [43], the authors believe that the exact moment of the transition was observed during this experiment. The numerical results for this case do not show the same "peak appearance", but the nature of the function sequence is similar.

For ΔT = 11 °C, the experimental results are similar to the smaller temperature difference case. The black line presenting the natural convection behavior is almost linear, having a good match to the $-5/3$ exponent of the power law (a pink dashed line) and is positioned lower than the functions for the thermo-magnetic convection. For $\mathbf{b}_{0MAX}$ = 1T (the red line), the function is still quite straight but it moves upwards indicating a change. For this case the Rayleigh number is 2.2×10^5 and the thermo-magnetic Rayleigh number is 1.43×10^7; taking into account the analyses from Figures 5 and 7 and that in [44] Akashi reports that the convective motion is approaching the state of fully developed turbulence for $Ra = 1.8 \times 10^5$, the authors believe this to be the point of transition from the laminar to turbulent flow, especially since for the numerical results (Figure 9b) a peak is clearly visible on the red line (for frequencies 0.0499 and 0.0599). From the presented power spectra one other conclusion can be drawn—the inertial range is elongated with the increasing magnetic field strength, which indicates that the energy transport mechanism changes and in the higher magnetic field values the energy that is transported mostly by the moving fluid and only for the highest frequency values is the energy dissipated by molecular viscosity.

Exemplary results of the wavelet analysis are shown in Figures 10 and 11 for ΔT = 5 °C and ΔT = 11 °C respectively. The upper panel shows the values of the wavelet transform function and the lower panel for the original temperature fluctuations.

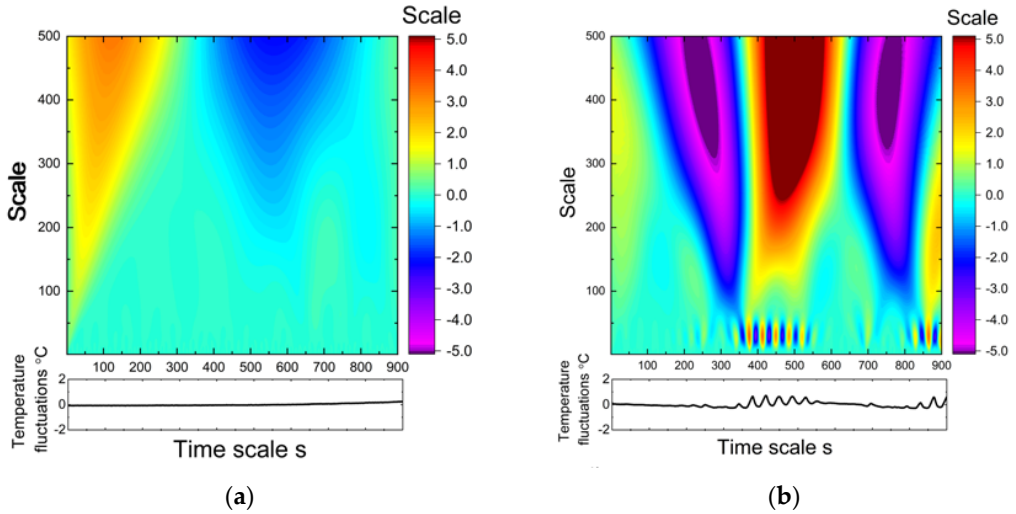

Figure 10. Wavelet analysis of the for the case with ΔT = 5 °C and magnetic induction of (**a**) 1T and (**b**) 2T.

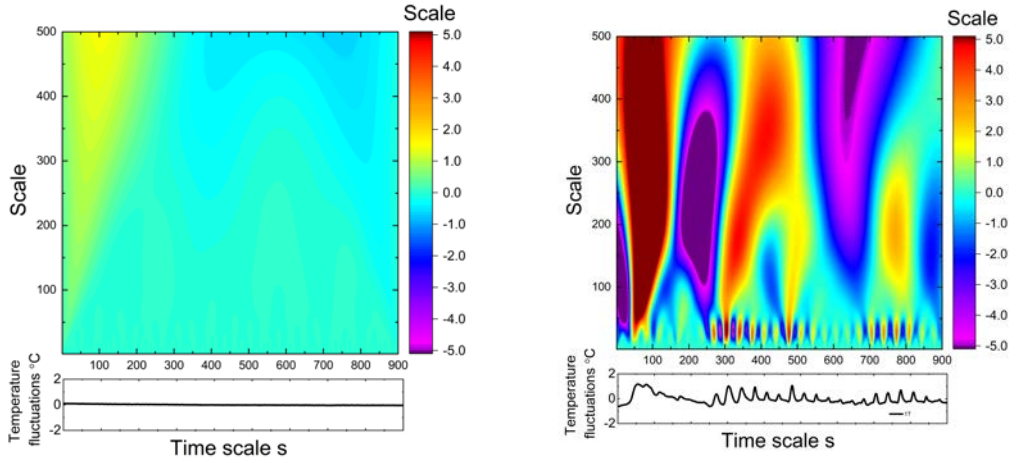

Figure 11. Wavelet analysis of the for the case with ΔT = 11 °C and magnetic induction of (**a**) 0T and (**b**) 1T.

For the smaller temperature difference, the cases with the magnetic induction of 1T and 2T were selected. For the case with $\mathbf{b}_{0MAX}$ = 1T, the colormap presents mostly azure color (values near 0) and only two areas for the large scales—yellow-orange in the upper left corner and dark blue in the middle-right upper part can be observed. Those two regions suggest small and slow deviation from the mean temperature indicating that the flow is steady and laminar. After introducing the magnetic field of 1T to the system, the character on the colormap changes greatly—small red/blue structures appear at the bottom and large, plumelike areas for the larger scales. The disorganized field near the bottom contributes primarily to the background turbulence at the small scales (under 50 s). These structures are characterized by strong positive centers in red and deep negative centers in violet, which occur alternatively. For larger scales they tend to merge to three distinctive structures, which we believe represent the low-frequency large eddies or thermal plumes penetrating the entire enclosure.

For the larger temperature difference (Figure 11) the wavelet colormaps are presented for the natural convection case (no magnetic induction) and for $\mathbf{b}_{0MAX}$ = 1T. Similar to the previous case, the wavelet map presenting the laminar steady flow is mostly uniform and wavelet coefficients are close to 0. Significant changes occur after applying the magnetic field of 1T, and therefore changing the type of the flow from laminar to transient/turbulent. Many small structures appear at the bottom of the map reflecting the fluctuations presented in the lower panel. Those again are contributed primarily to the background turbulence at the very small scales (under 40 s). For scales over 40 s these small structures tend to merge to large plumelike areas representing greater tendencies in the flow. For example, the first plume from the left (the maroon color) is associated with the wide temperature fluctuation that takes place from thirty to one hundred seconds and has a temperature value above the mean. Those high, pronounced structures represent large convective thermal plumes moving along the bottom surface in the experimental enclosure. Numerical visualizations of the flow field confirm this phenomenon which verifies the use of the wavelet transform as a visualization tool in the experimental cases where the traditional methods to envision the thermal flow field are not applicable.

6.2. Velocities

As the experimental analysis does not allow for the measuring of the velocity of the fluid in the experimental enclosure, the velocity analysis was conducted only based on the numerical results.

Figure 12 presents the horizontal (u) and vertical (v) components of the velocity fluctuations for (a) ΔT = 5 °C and (b) with ΔT = 11 °C for the natural convection case

($\mathbf{b}_{0MAX}$ = 0T) and for $\mathbf{b}_{0MAX}$ = 1–6.9T. For both temperature differences it can be observed that the increasing magnetic field induction creates an enlargement of the velocity fluctuations. For smaller temperature differences for the neutral case the mean horizontal and vertical velocities are 1.26×10^{-5} m/s and 1.88×10^{-4} m/s, respectively, while for the maximal value of the magnetic induction ($\mathbf{b}_{0MAX}$ = 9T) it is 5.95×10^{-4} m/s and 2.93×10^{-4} m/s. For the larger temperature differences the increase of the mean velocity is even higher—from 1.42×10^{-4} m/s and 2.55×10^{-4} m/s for natural convection to 1.31×10^{-3} m/s and 5.51×10^{-4} m/s for $\mathbf{b}_{0MAX}$ = 9T for the horizontal and vertical part, respectively. It proves the enhancing effect of the magnetic field on the convection.

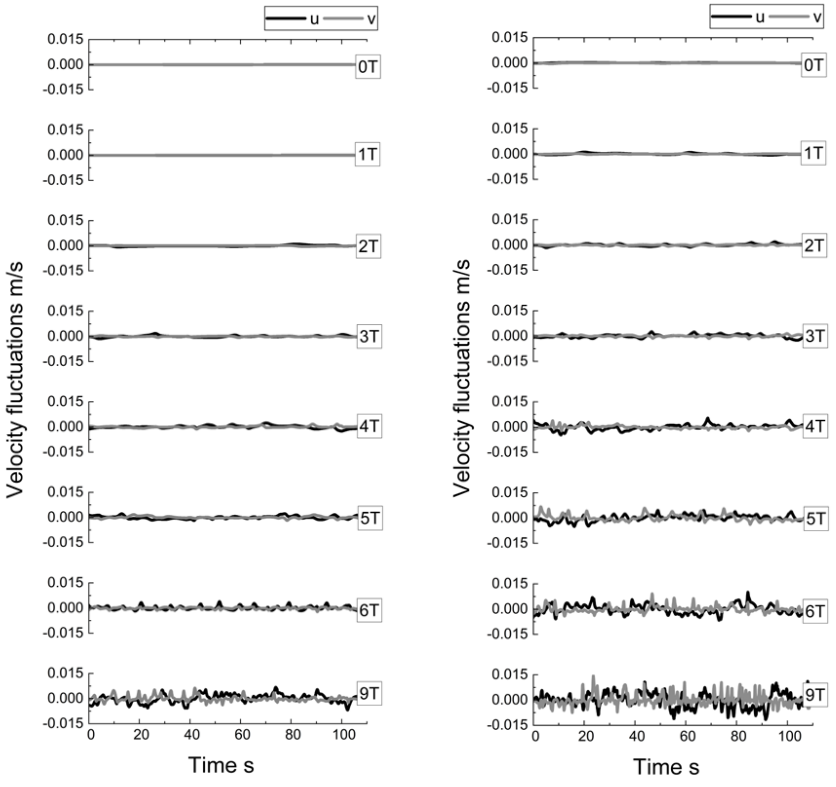

(**a**) (**b**)

Figure 12. Velocity fluctuations for the numerical case with (**a**) ΔT = 5 °C and (**b**) ΔT = 11 °C.

The FFT analysis for the velocity signals is presented in Figures 13–16 as n amplitude-frequency graph and power spectrum. To maintain transparency, only a chosen result will be presented: for ΔT = 5 °C: $\mathbf{b}_{0MAX}$ = 0, 2, 5, 9T and for ΔT = 11 °C: $\mathbf{b}_{0MAX}$ = 0, 1, 5, 9T.

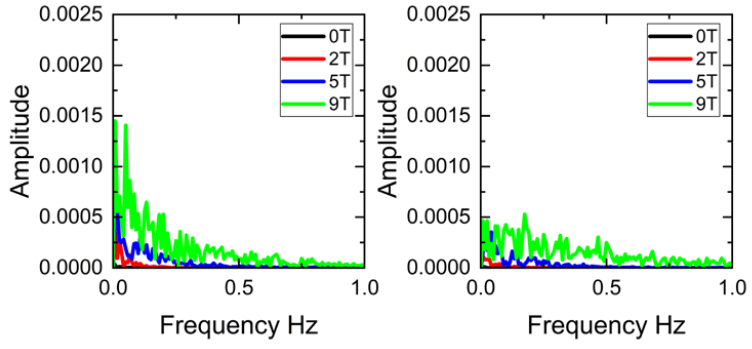

(**a**) (**b**)

Figure 13. Fast Fourier transform results for the velocity components u (**a**) and v (**b**) for the case with ΔT = 5 °C.

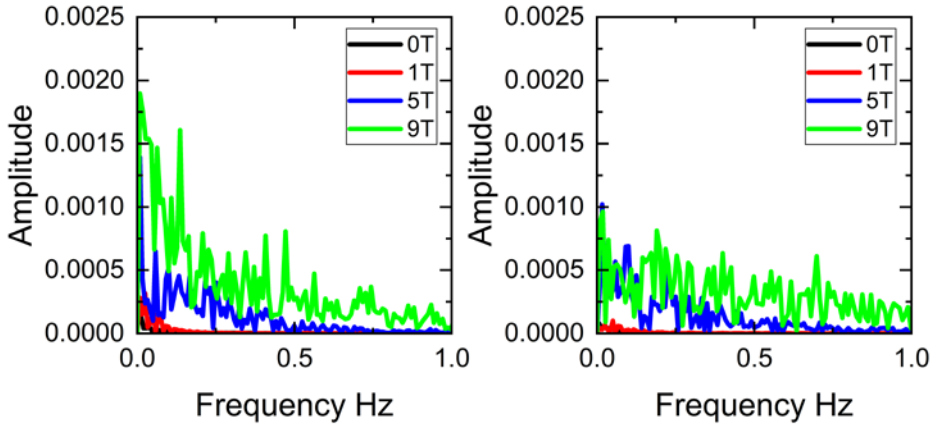

Figure 14. Fast Fourier transform results for the velocity components u (**a**) and v (**b**) for the case with ΔT = 11 °C.

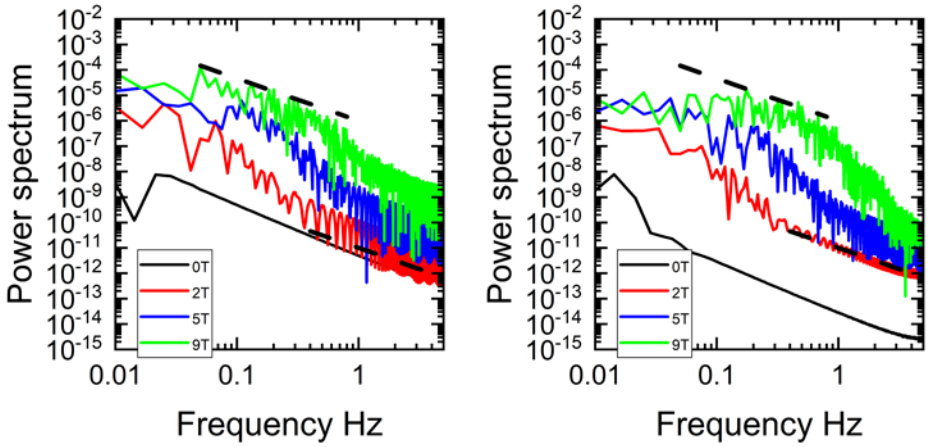

Figure 15. Power spectrum for the velocity components u (**a**) and v (**b**) for the case with ΔT = 5 °C.

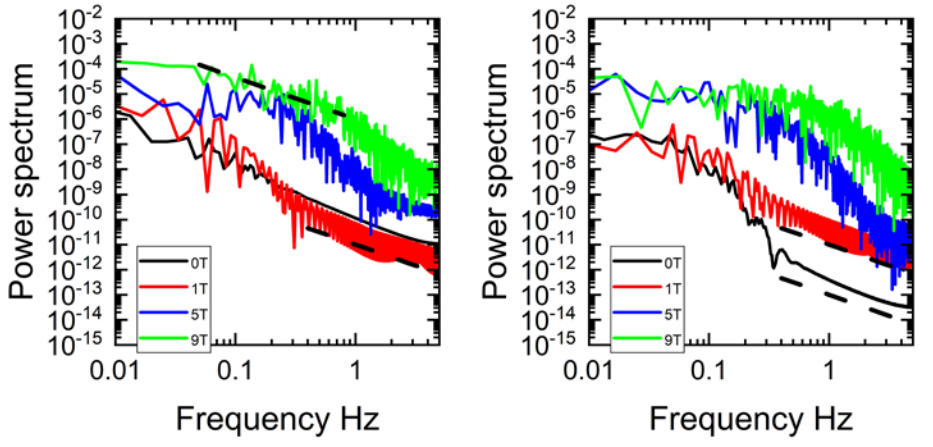

Figure 16. Power spectrum for the velocity components u (**a**) and v (**b**) for the case with ΔT = 11 °C.

Figure 13 presents amplitude versus frequency for the numerical analyses for the horizontal (u) and vertical (v) components of the velocity for the temperature difference

of 5 °C. For the neutral case there are no visible peaks on the graphs, suggesting that the flow is steady and laminar. For $\mathbf{b}_{0MAX}$ = 2T, two characteristic frequencies with low amplitudes can be observed (0.0083 Hz and 0.0249 Hz). A further increase of the imposed magnetic induction shows a growing amplitude tendency, with the maximum magnitude of amplitude for $\mathbf{b}_{0MAX}$ = 9T. Specific frequencies for this case are 0.0083, 0.1332, 0.1998 Hz and 0.0083, 0.0249, 0.1748 Hz for the horizontal and vertical parts, respectively.

For the higher temperature difference results, presented in Figure 14, one visible peak for the neutral case can be observed for the horizontal velocity (0.0066 Hz). After applying magnetic induction to the system, four characteristic frequencies can be observed for $\mathbf{b}_{0MAX}$ = 1T: 0.0083, 0.0249, 0.0499, and 1.3484 Hz. A further increase of the imposed magnetic induction shows a growing amplitude of the observed peaks and a tendency to widen the spectrum—a more continuous spectrum with a wide range of specific frequencies—this is a phenomenon typical of a well-developed turbulence.

The power density of the velocity is shown in Figures 15 and 16. For the smaller temperature difference between the thermally active walls (Figure 15) for the natural convection case, the energy spectrum of the both velocity components has an almost linear type. This specific behavior changes with the application of the external magnetic field and with the temperature—as for $\mathbf{b}_{0MAX}$ = 0T and ΔT = 11 °C (Figure 16) the power density function is no longer smooth. For higher magnetic inductions, as the flow changes its character from laminar to turbulent, the energy spectrum functions have more ragged characters. It is also visible that with the increase of the magnetic induction and the increasing velocity of the fluid, the power density function is shifting towards higher energies. The inertial range is elongated and the function lines tend to bulge slightly. For lower values of the magnetic inductions and higher frequencies, a good match to the $-5/3$ exponent law (the dashed line) can be observed, especially for the transitional case (2T). This clearly indicates that the kinetic energy is transmitted from the larger scales to smaller vortices and then dissipated according to the Kolmogorov theory.

Figures 17 and 18 presents selected temperature colormaps with fluid streamlines and normalized velocity vectors (for ΔT = 5 °C vector are scaled $\times 2$ in comparison to the ΔT = 11 °C case). For the natural convection cases ($\mathbf{b}_{0MAX}$ = 0T) for the smaller temperature difference, a small thermal plume of hot fluid on the middle-right part at the bottom and a cold fluid plume diagonally with up and downdrafts at the sidewalls can be observed along with the stream traces. The observed plumes have wide and thick stems with no distinct heads which is explainable by the both wide thermal and velocity boundary layers. The homogenization of the temperature around the plumes and barely visible velocity vectors point to a strong diffusion component in the natural convection case. With the increase of the magnetic induction—for $\mathbf{b}_{0MAX}$ = 2T those budding thermal structures develop and traces of the fluid emerging from thermal plumes are expanding. Those flow structures differ significantly in comparison to the results presented in [32], where the authors reported one central hot-fluid plume in the center of the cubical enclosure for the neutral case (without magnetic induction). It appears that the lower geometry favors the desymmetrization of the flow structure. For higher magnetic field values the observed plumes tend to narrow and lengthen penetrating almost the entire height of the enclosure ($\mathbf{b}_{0MAX}$ = 5T) which is in accordance with [32]. It is a classic example of a viscous-non diffusive flow regime, which is defined by thin temperature boundary layers and thick velocity boundary layers and results in plumes with a thin stem and well defined head with side lobes. The velocity dissipation occurs by viscous friction rather than by vortices. As this regime exists for moderate Rayleigh numbers ($10^5 < Ra < 10^6$), the Prandtl numbers over 10 [45] and the very fine grids are required to capture the mentioned dynamics. This thermal plume behavior was not observed in the publications mentioned in the introductory section.

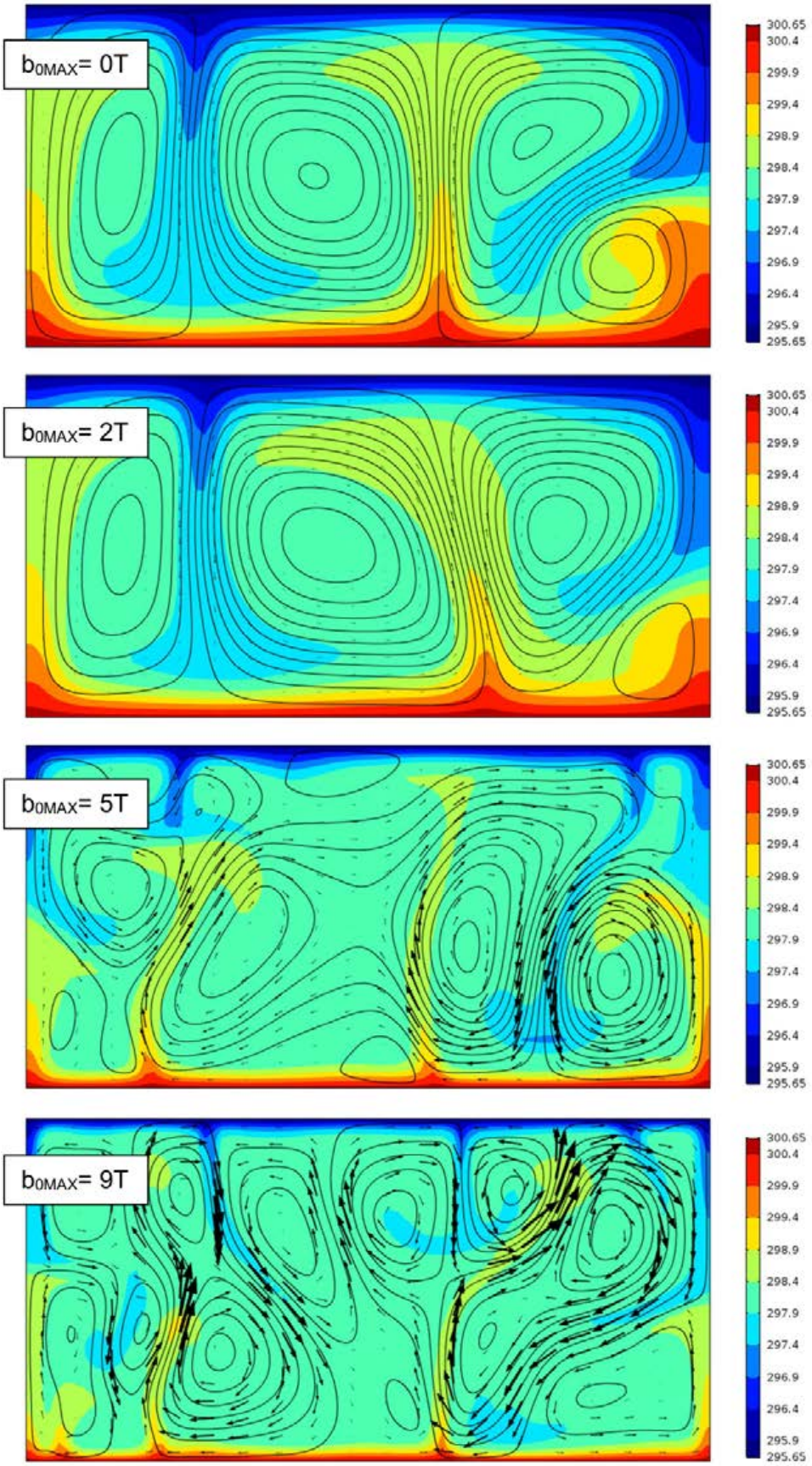

Figure 17. Temperature color maps with stream lines and velocity vectors for numerical simulations for $\Delta T = 5$ °C. The velocity vectors are scaled $\times 2$ in comparison to Figure 18.

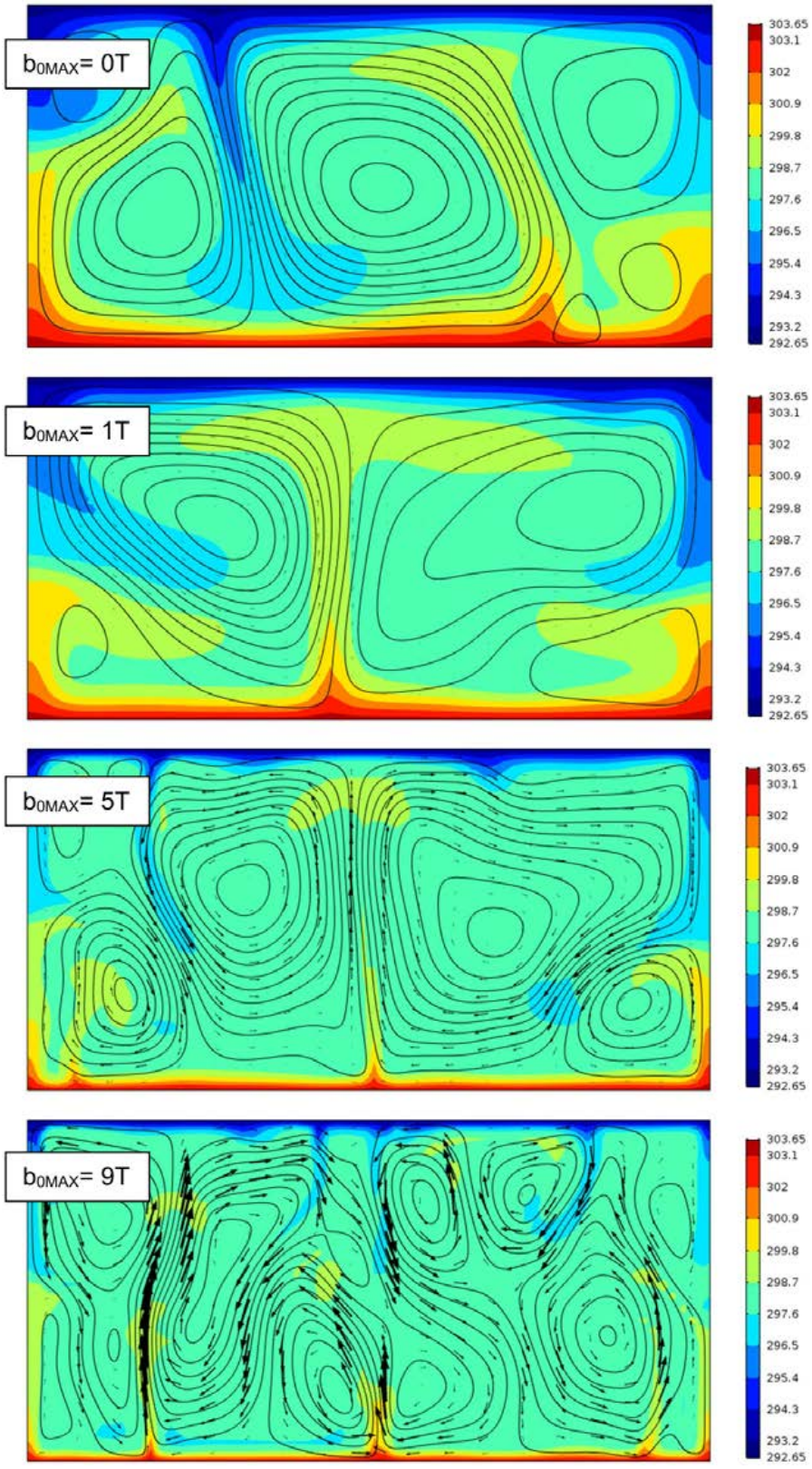

Figure 18. Temperature color maps with stream lines and velocity vectors for numerical simulations for $\Delta T = 11$ °C.

An interesting difference emerges for the highest magnetic field strength. In the presented study a kind of a "dissection" of the flow can be observed. Two rows of coherent structures appear with six clear rotating structures separated by "mushroom-like" plumes

in the top section. It is also a characteristic behavior for another flow regime called inviscid-non diffusive, which is defined by both thin temperature and velocity boundary layers. With simulation time, the observed plume's stems become sinusoidal and alternating vortices are shed from either side of the thermal lobes, pointing to the fact that energy is no longer dissipated by the viscous friction but by the vortices. This disintegration of a whole length plume to a two row structure is a result of intense turbulent mixing in the flow ($\mathbf{b}_{0MAX}$ = 9T).

For higher temperature differences the process is similar. After applying magnetic induction to the system, there is an intense meandering of thermal plums both on the top and bottom surfaces, and the process of lengthening of plumes occurs faster with higher temperature differences. At the stronger magnetic inductions there are intensive run ups and downs at the vertical walls (the wall heat transfer regime reported by [42]). The flow structure for the highest value of the magnetic field presents a model picture of turbulence—with high velocity vectors, thermal plumes meandering on the active surfaces and dissipating as a result of the intensity of the flow. This obtained flow field is almost identical to the results presented in [46] for Prandtl number 100 and Ra = 5.4 × 10^9 (Prandtl number in ΔT = 11 °C is equal to 98.7 and Ra_{TM} = 1.12 × 10^9). Therefore, it can be concluded that the strong magnetic field applied to the paramagnetic fluid can accelerate the full turbulence formation in comparison to free convection without changing the thermal conditions of the system.

Figure 19 presents the changes of the Nusselt number with time and magnetic field induction for the numerical analysis for both temperature differences. For both cases it can be clearly seen that the increase in magnetic induction causes a significant change in heat transfer in the system—the Nusselt number grows. For ΔT = 5 °C, the mean values of Nu for $\mathbf{b}_{0MAX}$ = 0T and 1T are 4.36 and 4.63 respectively. For the magnetic induction of 2T it changes notably to 5.41—this is caused by the magnetic field influence on the fluid flow character. As the flow changes from laminar to transient and turbulent, the heat transfer is intensified. Further enhancing of the magnetic induction produces enlargement of the Nusselt number and for the $\mathbf{b}_{0MAX}$ = 9T and Ra_{TM} = 5.15 × 10^8 a rapid, oscillatory character of changes in time can be observed. It is connected with the additional wall-heat transfer as reported by the [42].

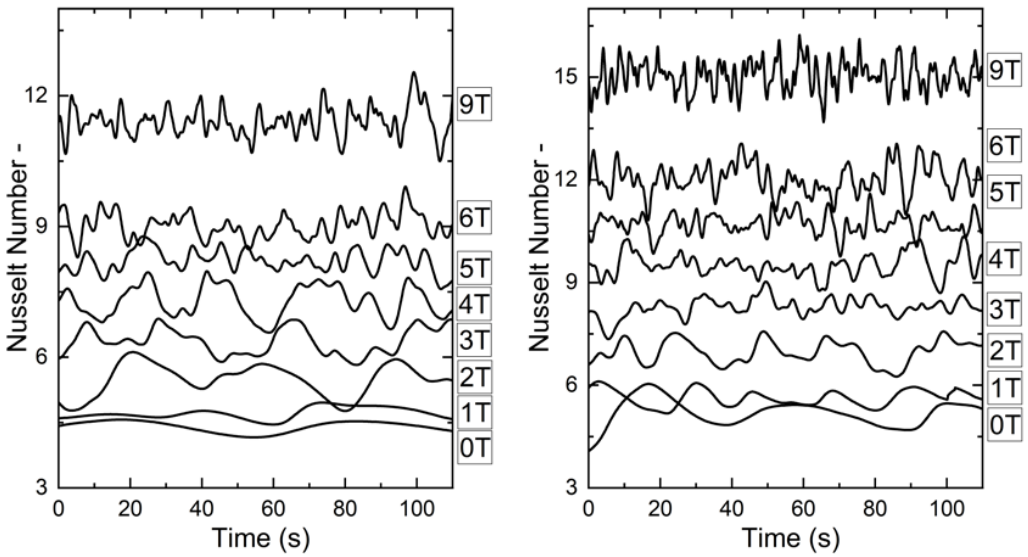

Figure 19. Changes of the Nusselt number with time for the numerical case with (**a**) ΔT = 5 °C and (**b**) ΔT = 11 °C.

For the larger temperature difference (Figure 19b) the same tendencies can be observed, with the exception that the significant influence of the magnetic field induction

on the heat transfer in the system is already visible for the first two cases $\mathbf{b}_{0MAX}$ = 0T and 1T—the mean value of the Nu number changes from 5.12 to 5.55. Also, the oscillatory character of the Nusselt number in time can be seen for smaller values of the magnetic induction, which corresponds to the oscillatory regime named by [43]: for $\mathbf{b}_{0MAX}$ = 5T and $Ra_{TM} = 3.48 \times 10^8$ Nu = 10.2, for $\mathbf{b}_{0MAX}$ = 6T and $Ra_{TM} = 5.06 \times 10^8$ Nu = 11.4, and for $\mathbf{b}_{0MAX}$ = 9T and $Ra_{TM} = 1.12 \times 10^9$ Nu = 15.

7. Summary

An analysis of the natural convection of a paramagnetic fluid in the strong external magnetic field for shallow geometry was presented. The emphasis of this research was placed on the changes in the flow structure under different magnetic field strengths, but the enhancement of the heat transfer in the system was also analyzed.

Experimental and numerical data were analyzed with the application of the fast Fourier transform, which granted designation of the specific frequencies of the fluid flow and also made it possible to observe the changes in the character of the temperature spectral function and power density, especially under the conditions where the flow changes from laminar to turbulent. It was proven that the magnetic field applied to the paramagnetic, one-phase fluid flow elongates the inertial regime of the flow. A Wavelet analysis of the experimental results, as a new analytical method in the thermo-magnetic field, allowed—to some extent—visualization of the process, which is not possible in our laboratory conditions.

The presented results and their analysis indicate that the transition from laminar to turbulent character of the flow in a geometry with a smaller aspect ratio than 1 occurs for $Ra_{TM} = 2.58 \times 10^7$ in a case with ΔT = 5 °C, and for $Ra_{TM} = 1.43 \times 10^7$ for ΔT = 11 °C, which is compatible with the conclusions in [42] for cubical geometry, and is in near agreement with [33]. Further research, involving geometries with a greater range of aspect ratios, is needed to determine an accurate scale for laminar-turbulent transition in thermo-magnetic convection.

The numerical results of the presented phenomena and the obtained temperature-stream lines maps from the 2D simulations performed on a dense grid allow precise observation of thermal plume evolution with increasing dynamization of the flow—from a diffusive-viscous regime, via a viscous-non diffusive regime, up to an inviscid-non diffusive region, where energy can no longer be dissipated though viscous shear.

The heat transfer analysis showed that the Nusselt number value increases over 260% for smaller temperature differences and almost by 300% for ΔT = 11 °C for the highest magnetic field value.

This research paper provides new findings on the matter of the laminar-turbulent flow transition in paramagnetic, one-phase fluids subjected to an external magnetic field, and can be used to build a benchmark for the next analysis of this phenomenon. Further plans to obtain a comprehensive scheme to analyze both experimental and numerical data in the thermo-magnetic field of research is to utilize a proper orthogonal decomposition—a method allowing a capture of the turbulence intensity with regard to the components of the flow.

Author Contributions: Conceptualization, A.K. and J.D.; methodology, A.K. and J.D.; validation, A.K. and J.D.; A.K. and J.D.; investigation, A.K. and J.D.; writing—original draft preparation, A.K. and J.D.; visualization, A.K. and J.D.; supervision, J.D.; funding acquisition, J.D. All authors have read and agreed to the published version of the manuscript.

Funding: This work was supported by the Polish Ministry of Science and Higher Education (grant AGH no. 16.16.210.476) and by the National Science Centre (Project No. 12/07/B/ST8/03109).

Institutional Review Board Statement: Not applicable.

Informed Consent Statement: Not applicable.

Data Availability Statement: Data available on reasonable request.

Conflicts of Interest: The authors declare no conflict of interest. The funders had no role in the design of the study; in the collection, analyses, or interpretation of data; in the writing of the manuscript, or in the decision to publish the results.

Nomenclature

a	base dimension of the experimental enclosure (m)
a	shape parameter in wavelet function (-)
$\mathbf{b}_{0\max}$	magnetic induction in the center of the magnet (T)
b	location parameter in wavelet function (-)
$C_{a,b}$	wavelet coefficient (-)
c_p	heat capacity (J/kgK)
d	height (m)
$\mathbf{f^g}$	gravitational force (N/m^3)
$\mathbf{f^G}$	gravitational buoyancy force (N/m^3)
$\mathbf{f^{mg}}$	magnetic force (N/m^3)
$\mathbf{f^{MG}}$	magnetic buoyancy force (N/m^3)
F_n	discrete Fourier function (-)
g	gravitational acceleration (m^2/s)
H	intensity of a magnetic field (A/m)
k	wave number (-)
M	magnetization (A/m)
n**n**	length of sequence i (-)normal vector to the sphere surface (-)
$Q_{\text{net\_cond}}$	net conduction heat flux (W)
$Q_{\text{net\_conv}}$	net convection heat flux (W)
t	time (s)
T	temperature (°C)
T_0	reference temperature (°C)
T_h	temperature at the heated wall (°C)
T_c	temperature at the cooled wall (°C)
x_i	sequence length (-)
Imaginary	imaginary part of transformed data (-)
Real	real part of transformed data (-)
α	thermal diffusivity (m^2/s)
β	thermal expansion coefficient (1/K)
λ	thermal conductivity (W/mK)
μ_0	magnetic permeability of vacuum (H/m)
μ	dynamic viscosity (kg/ms)
ν	kinematic viscosity (m^2/s)
ρ	density (kg/m^3)
χ_m	mass magnetic susceptibility (m^3/kg)
χ	volume magnetic susceptibility (-)
$\text{Nu} = Q_{\text{net\_conv}}/Q_{\text{net\_cond}}$	Nusselt number (-)
$\text{Ra}_T = \frac{\mathbf{g}\beta(T_h - T_c)d^3}{\alpha\nu}$	thermal Rayleigh number (-)
$\text{Ra}_M = \left(1 + \frac{1}{\beta T_0}\right)\left[\frac{\mathbf{g}\gamma\beta(T_h - T_c)d^3}{2\alpha\nu}\right]$	magnetic Rayleigh number (-)
$\text{Ra}_{TM} = \text{Ra}_T + \text{Ra}_M$	thermo-magnetic Rayleigh number (-)
$\gamma = \frac{\chi\lvert b_0\rvert^2_{\max}}{\rho\mu_m \mathbf{g}d}$	magnetization number (-)

References

1. Lord Rayleigh, O.M. On Convection Currents in a Horizontal Layer of Fluid, When the Higher Temperature Is on the under Side. *Lond. Edinb. Phil. Mag.* **1916**, *32*, 529–546. [CrossRef]
2. *The Bénard (1900, 1901) Convection Problem, Heated from Below*; Springer: New York, NY, USA, 2009. [CrossRef]
3. Dropkin, D.; Somerscales, E. Heat Transfer by Natural Convection in Liquids Confined by Two Parallel Plates Which Are Inclined at Various Angles with Respect to the Horizontal. *J. Heat Transf.* **1965**, *87*, 77–82. [CrossRef]

4. Somerscales, E.F.C.; Dropkin, D. Experimental Investigation of the Temperature Distribution in a Horizontal Layer of Fluid Heated from Below. *Int. J. Heat Mass Transf.* **1966**, 1189–1204. [CrossRef]
5. Heslot, F.; Castaing, B.; Libchaber, A. Transitions to Turbulence in Helium Gas. *Phys. Rev. A* **1987**, *36*, 5870–5873. [CrossRef]
6. Silveston, P.L. Wärmedurchgang in Waagerechten Flüssigkeitsschlichten. *Forach. Geb. Ing. Ser. 8* **1968**, *24*, 29–32.
7. Whittaker, E.T. *A History of the Theories of Aether and Electricity from the Age of Descartes to the Close of the Nineteenth Century*; Thomas Nelson and Sons Ltd.: London, UK, 1910.
8. Faraday, M. On the Diamagnetic Conditions of Flame and Gases. *Lond. Edinb. Phil. Mag.* **1847**, *31*, 401–421. [CrossRef]
9. Wu, M.K.; Ashburn, J.R.; Torng, C.J.; Hor, P.H.; Meng, R.L.; Gao, L.; Huang, Z.J.; Wang, Y.Q.; Chu, C.W. Superconductivity at 93 K in a New Mixed-Phase Y-Ba-Cu-O Compound System at Ambient Pressure. *Phys. Rev. Lett.* **1987**, *58*, 908. [CrossRef]
10. Braithwaite, D.; Beaugnon, E.; Tournier, R. Magnetically Controlled Convection in a Paramagnetic Fluid. *Nature* **1991**, *354*, 134–136. [CrossRef]
11. Huang, J.; Edwards, B.; Gray, D. Magnetic Control of Convection in Nonconducting Paramagnetic Fluids. *Phys. Rev. E* **1998**, *57*, 29. [CrossRef]
12. Ozoe, H. *Magnetic Convection*; Imperial College Press: London, UK, 2005; pp. 1–224. [CrossRef]
13. Tagawa, T. Numerical Simulation of Two-Phase Flows in the Presence of a Magnetic Field. *Math. Comput. Simul.* **2006**, *72*, 212–219. [CrossRef]
14. Tagawa, T.; Ujihara, A.; Ozoe, H. Numerical Computation for Rayleigh–Benard Convection of Water in a Magnetic Field. *Int. J. Heat Mass Transf.* **2003**, *46*, 4097–4104. [CrossRef]
15. Tagawa, T.; Shigemitsu, R.; Ozoe, H. Magnetizing Force Modeled and Numerically Solved for Natural Convection of Air in a Cubic Enclosure: Effect of the Direction of the Magnetic Field. *Int. J. Heat Mass Transf.* **2002**, *45*, 267–277. [CrossRef]
16. Bednarz, T.; Patterson, J.C.; Lei, C.; Ozoe, H. Enhancing Natural Convection in a Cube Using a Strong Magnetic Field—Experimental Heat Transfer Rate Measurements and Flow Visualization. *Int. Commun. Heat Mass Transf.* **2009**, *36*, 781–786. [CrossRef]
17. Bednarz, T.; Fornalik, E.; Tagawa, T.; Ozoe, H. Convection of Paramagnetic Fluid in a Cube Heated and Cooled from Side Walls and Placed below a Superconducting Magnet. *Therm. Sci. Eng.* **2006**, *14*, 107–114.
18. Bednarz, T.P.; Lei, C.; Patterson, J.C.; Ozoe, H. Effects of a transverse, horizontal magnetic field on natural convection of a paramagnetic fluid in a cube. *Int. J. Therm. Sci.* **2009**, *48*, 26–33. [CrossRef]
19. Wrobel, W.; Fornalik-Wajs, E.; Szmyd, J.S. Experimental and Numerical Analysis of Thermo-Magnetic Convection in a Vertical Annular Enclosure. *Int. J. Heat Fluid Flow* **2010**, *31*, 1019–1031. [CrossRef]
20. Postelnicu, A. Influence of a Magnetic Field on Heat and Mass Transfer by Natural Convection from Vertical Surfaces in Porous Media Considering Soret and Dufour Effects. *Int. J. Heat Mass Transf.* **2004**, *47*, 1467–1472. [CrossRef]
21. Fornalik, E.; Filar, P.; Tagawa, T.; Ozoe, H.; Szmyd, J.S. Effect of a Magnetic Field on the Convection of Paramagnetic Fluid in Unstable and Stable Thermosyphon-like Configurations. *Int. J. Heat Mass Transf.* **2006**, *49*, 2642–2651. [CrossRef]
22. Huang, C.S.; Yu, C.W.; Chen, R.H.; Tzeng, C.T.; Lai, C.M. Experimental Observation of Natural Convection Heat Transfer Performance of a Rectangular Thermosyphon. *Energies* **2019**, *12*, 1702. [CrossRef]
23. Pleskacz, L.; Fornalik-Wajs, E. Magnetic Field Impact on the High and Low Reynolds Number Flows. *J. Phys. Conf. Ser.* **2014**, *530*, 1–12. [CrossRef]
24. Roszko, A.; Fornalik-Wajs, E. Magnetic Nanofluid Properties as the Heat Transfer Enhancement Agent. In *E3S Web of Conferences*; EDP: Les Ulis, France, 2016; p. 00111.
25. Hiba, B.; Redouane, F.; Jamshed, W.; Ahamed Saleel, C.; Suriya Uma Devi, S.; Prakash, M.; Nisar, K.S.; Vijayakumar, V.; Eid, M.R. A Novel Case Study of Thermal and Streamline Analysis in a Grooved Enclosure Filled with (Ag–MgO/Water) Hybrid Nanofluid: Galerkin FEM. *Case Stud. Therm. Eng.* **2021**, *28*, 101372. [CrossRef]
26. Selimefendigil, F.; Oztop, H.F.; Sheremet, M.A.; Abu-Hamdeh, N. Forced Convection of Fe3O4-Water Nanofluid in a Bifurcating Channel under the Effect of Variable Magnetic Field. *Energies* **2019**, *12*, 666. [CrossRef]
27. Bagheri, H.; Behrang, M.; Assareh, E.; Izadi, M.; Sheremet, M.A. Free Convection of Hybrid Nanofluids in a C-Shaped Chamber under Variable Heat Flux and Magnetic Field: Simulation, Sensitivity Analysis, and Artificial Neural Networks. *Energies* **2019**, *12*, 2807. [CrossRef]
28. Salleh, S.N.A.; Bachok, N.; Arifin, N.M.; Md Ali, F.; Pop, I. Magnetohydrodynamics Flow Past a Moving Vertical Thin Needle in a Nanofluid with Stability Analysis. *Energies* **2018**, *11*, 3297. [CrossRef]
29. Szabo, P.S.B.; Früh, W.G. The Transition from Natural Convection to Thermomagnetic Convection of a Magnetic Fluid in a Non-Uniform Magnetic Field. *J. Magn. Mater.* **2018**, *447*, 116–123. [CrossRef]
30. Kenjereš, S.; Pyrda, L.; Fornalik-Wajs, E.; Szmyd, J.S. Numerical and Experimental Study of Rayleigh–Bénard–Kelvin Convection. *Flow Turbul. Combust.* **2014**, *92*, 371–393. [CrossRef]
31. Pyrda, L.; Kenjeres, S.; Fornalik-Wajs, E.; Szmyd, J.S. An Analysis of Unsteady Thermal Convection of Paramagnetic Fluid in Cubical Enclosure under Strong Magnetic Field Gradient. *J. Phys. Conf. Ser.* **2012**, *395*, 012125. [CrossRef]
32. Kenjereš, S.; Wrobel, W.; Pyrda, L.; Fornalik-Wajs, E.; Szmyd, J.S. Transients and Turbulence Pockets in Thermal Convection of Paramagnetic Fluid Subjected to Strong Magnetic Field Gradients. *J. Phys. Conf. Ser.* **2011**, *318*, 072028. [CrossRef]
33. Pyrda, L.; Kraszewska, A. Experimental Thermo-Magnetic Convection Analysis in Tall Rectangular Enclosure. *J. Phys. Conf. Ser.* **2016**, *745*, 032155. [CrossRef]

34. Kraszewska, A.; Pyrda, L.; Donizak, J. High Magnetic Field Impact on the Natural Convection Behaviour of a Magnetic Fluid. *Heat Mass Transf.* **2018**, *54*, 2383–2394. [CrossRef]
35. Zeytounian, R.K. Joseph Boussinesq and His Approximation: A Contemporary View. *Comptes Rendus Mec.* **2003**, *331*, 575–586. [CrossRef]
36. Ozoe, H.; Churchill, S.W. Hydrodynamic Stability and Natural Convection in Newtonian and Non-Newtonian Fluids Heated from Below. *AIChE Sympos. Ser. Heat Transf.* **1973**, *69*, 126–133.
37. Mattis, D.C. *The Theory of Magnetism Made Simple: An Introduction to Physical Concepts and to Some Useful Mathematical Methods*; World Scientific: Singapore, 2006; pp. 1–567. [CrossRef]
38. Help Online—Origin Help—Fast Fourier Transform (FFT). Available online: https://www.originlab.com/doc/Origin-Help/FFT (accessed on 18 October 2021).
39. Elsner, J.W. *Turbulencja Przepływów (Turbulence of Flows)*; Państwowe Wydawnictwo: Naukowe, Warszawa, 1987.
40. Morlet, J.; Arens, G.; Fourgeau, E.; Giard, D. Wave Propagation and Sampling Theory—Part II. Sampling Theory and Complex Waves. *Geophysics* **1982**, *47*, 222–236. [CrossRef]
41. Farge, M. Wavelet Transforms and Their Applications to Turbulence. *Annu. Rev. Fluid Mech.* **1992**, *24*, 395–458. [CrossRef]
42. Kenjereš, S.; Pyrda, L.; Wrobel, W.; Fornalik-Wajs, E.; Szmyd, J. Oscillatory States in Thermal Convectin of a Paramagnetic Fluid in a Cubical Enclosure Subjected to a Magnetic Field Gradient. *Phys. Rev. E* **2012**, *85*, 1–8. [CrossRef]
43. Pyrda, L. An Analysis of Magnetic Field Influence on Transient Regime between Laminar and Turbulent Convection. Ph.D. Thesis, AGH University of Science and Technology, Kraków, Poland, 2013.
44. Akashi, M.; Yanagisawa, T.; Tasaka, Y.; Vogt, T.; Murai, Y.; Eckert, S. Transition from Convection Rolls to Large-Scale Cellular Structures in Turbulent Rayleigh-Bénard Convection in a Liquid Metal Layer. *Phys. Rev. Fluids* **2019**, *4*, 033501. [CrossRef]
45. Lappa, M. The Dynamics of Thermal Plumes and Related Regimes of Motion. *Therm. Convect.* **2009**, 195–213. [CrossRef]
46. Yang, H.; Wei, Y.; Zhu, Z.; Dou, H.; Qian, Y. Statistics of Heat Transfer in Two-Dimensional Turbulent Rayleigh-Bénard Convection at Various Prandtl Number. *Entropy* **2018**, *20*, 582. [CrossRef] [PubMed]